GEOPHYSICAL RESEARCH LETTERS, VOL. 36, L07801, doi:10.1029/2008GL036797, 2009

Trends in solar spectral irradiance variability in the visible and infrared

Jerald W. Harder,[1] Juan M. Fontenla,[1] Peter Pilewskie,[1] Erik C. Richard,[1] and Thomas N. Woods[1]

Received 25 November 2008; revised 29 January 2009; accepted 3 March 2009; published 1 April 2009.

[1] The Spectral Irradiance Monitor (SIM) on-board the Solar Radiation and Climate Experiment (SORCE) satellite provides the first multi-year continuous measurements of solar spectral irradiance (SSI) variability from 200–2400 nm, accounting for about 97% of the total solar irradiance (TSI). In addition to irradiance modulation from active region passage, the SSI values for wavelengths with a brightness temperature greater than 5770 K show a brightening with decreasing solar activity, whereas those with lower brightness temperatures show a dimming. These results demonstrate that different parts of the solar atmosphere contribute differently to the TSI with the behavior in the deep photospheric layers giving an opposing and nearly compensating trend to that in the upper photospheric and lower chromospheric layers. These findings need to be incorporated into Earth-climate assessments since the solar forcing induced by these differential trends are inherently different from the relatively flat spectral contributions employed in the IPCC assessments. **Citation:** Harder, J. W., J. M. Fontenla, P. Pilewskie, E. C. Richard, and T. N. Woods (2009), Trends in solar spectral irradiance variability in the visible and infrared, *Geophys. Res. Lett.*, *36*, L07801, doi:10.1029/2008GL036797.

1. Introduction

[2] Based on a nearly 30-year record of uninterrupted, overlapping space-borne measurements, recent composites of TSI [*Fröhlich*, 2006; *Willson and Mordvinov*, 2003] demonstrate that the total solar radiative input into the Earth system increases by about 0.1% from solar minimum to solar maximum with larger variations on shorter time scales. While it is surmised that this change in the energy input is too small to account for all of the increases observed in global averaged temperature [*Forster et al.*, 2007] during the industrial age, recent work emphasizes the importance of SSI variability in understanding the Earth climate system. Starting with ultraviolet data from the Upper Atmosphere Research Satellite (UARS) in 1991 [*London et al.*, 1993] studies by several groups [see *Labitzke et al.*, 2002, and references therein] demonstrated that solar cycle variations of ultraviolet radiation modulate the production of ozone in the upper stratosphere that affect wave propagation and stratospheric circulation. Although the vertical coupling between the stratosphere and troposphere is not well understood, the connection between the ultraviolet solar spectral variability and stratospheric processes has been established through these studies. The consequences of variability in the visible and infrared portions of the spectrum, however, are less well established and remain poorly understood. The works of Lean, Haigh, and others [e.g., *Lean*, 1991; *Haigh*, 1994] suggest that these spectral contributions are important but most general circulation and climate models assume that the spectral variability in the visible and IR follow similar trends to TSI. The SORCE SIM [*Rottman et al.*, 2005; *Harder et al.*, 2005] has produced the first continuous observations of trends in solar irradiance over the visible and near-infrared spectral regions for the majority of the descending phase of Solar Cycle 23.

2. Observations

[3] Measuring multi-year solar variability is predicated on our ability to measure systematic instrumental degradation trends and to separate them from the small and slowly varying solar signal (auxiliary material).[1] The SIM employs a measurement-based correction that compares two identical spectrometers in flight; one that is used for daily measurements (SIM A) and the other (SIM B) has only 22% of the accumulated exposure of SIM A. The only assumption in the analysis is that the prism transmission can be expressed as the product of an initial transmission (T_0) at the time of calibration (t_0) multiplied by a degradation factor expressed in a logarithmic form by defining the optical thickness of the absorbing material responsible for the prism degradation. The on-orbit time and wavelength dependent prism transmission, $T(\lambda, t)$, is given by:

$$T(\lambda, t) = T_0 e^{-\tau(\lambda, t-t_0)}$$

The time dependent attenuation of the degrading layer $\tau(\lambda, t)$ is independently evaluated at 60 wavelengths from low-noise ESR fixed wavelength experiments on both spectrometers to reconcile the SSI inferred by them. The τ dependency on time and wavelength can be separated into a strictly wavelength dependent part, $\kappa(\lambda)$, that can be interpreted as the absorbing material(s) opacity and a strictly time dependent part, $C(t)$, that can be interpreted as the effective thickness (column) of the accumulated absorbing material on the surface of the prisms that is different for the two spectrometers. Analysis of the 4-year time series of the ESR fixed wavelength experiment continually verifies the constancy of the values of κ at all

[1]Laboratory for Atmospheric and Space Physics, University of Colorado, Boulder, Colorado, USA.

0094-8276/09/2008GL036797$05.00

[1]Auxiliary materials are available in the HTML. doi:10.1029/2008GL036797.

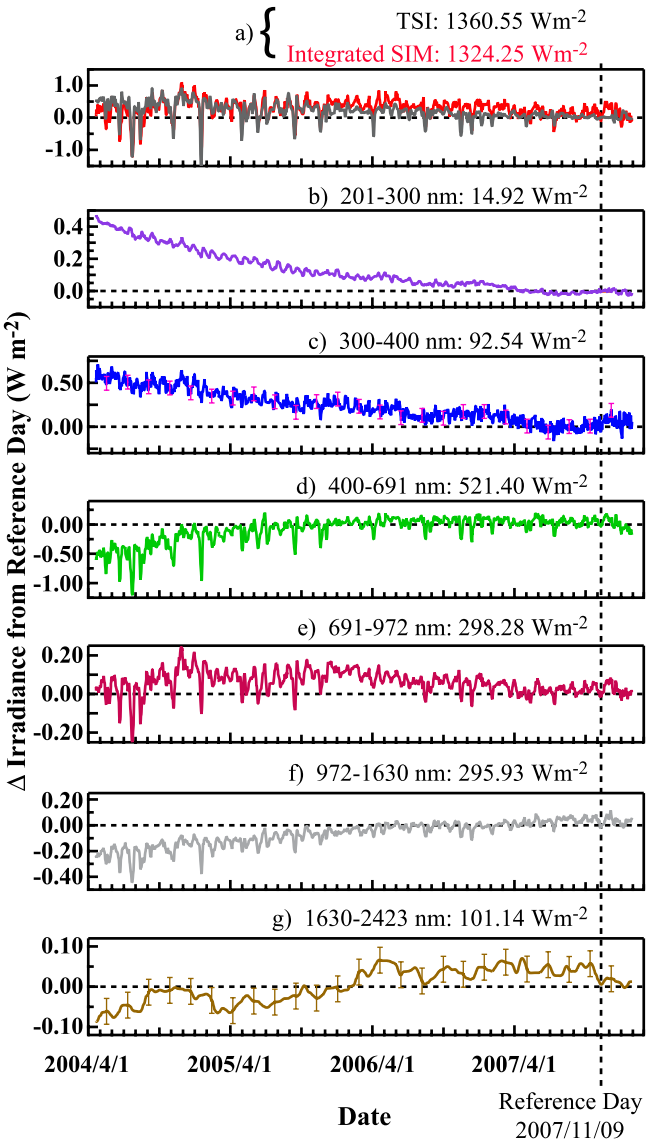

Figure 1. (a–g) The SIM spectral irradiance data integrated into discrete bands. The numerical values shown for each panel correspond to the average band integral during the 10-day period centered on 2007/11/09 of Solar Cycle 23 minimum-like conditions. The y-coordinate is the change in irradiance relative to this reference. The caption for each panel gives the integrated irradiance during the reference period. The 1630–2423 nm and 300–400 nm bands (Figures 1g and 1c, respectively) have a lower signal-to-noise ratio than the other bands where the noise is ~50 parts per million. The error bars in panel Figure 1g reflect the ~300 parts per million ($\pm 1\sigma$) uncertainty while those in Figure 1c correspond to ~900 parts per million ($\pm 1\sigma$).

wavelengths; and its value is refined to reflect the improved accuracy with which it can be defined from these comparisons over time. To date we have not found any significant change in kappa within the uncertainties of the method. The correction based strictly on exposure time tends to overestimate the degradation by about 0.2%; therefore at this point in the mission the value of $C(t)$ is adjusted to produce the same long-term trend in the integrated SIM data as seen in the TSI. This amounts to about a 4% change in the value of C different from what is obtained by the A/B comparisons alone and preserves the wavelength dependence of the degradation function.

[4] Figure 1 shows the time series of degradation-corrected SIM data integrated over six discrete bands spanning 200 to 2423 nm. Figure 1a shows the integrated SIM spectrum compared to the direct TSI measured by the SORCE Total Irradiance Monitor (TIM) [*Kopp et al.*, 2005]. The TSI value measured by TIM is 36.3 Wm^{-2} larger than the SIM integrated spectral irradiance because of contributions outside its measurement range; SIM accounts for 97.3% of the TSI. Excluding these unmeasured contributions, integrated SIM values agree with those from the TIM to 170 parts per million ($\pm 1\sigma$), demonstrating the effectiveness of the degradation corrections. In the wavelength regimes identified by Figures 1d and 1f the trends are out of phase with the TSI trend; conversely, in the 200–400 nm ultraviolet band (Figures 1b and 1c), the trend is in phase with the TSI. Figure 1e shows a relatively flat trend that is still affected by presence and decay of active regions.

[5] The offsetting irradiance trends seen in Figure 1 can be interpreted in terms of the SIM brightness temperature spectrum shown in Figure 2. For wavelengths where the effective brightness temperature is greater (less) than T_{eff} = 5770 K, the irradiance increases (decreases) with decreasing solar activity. T_{eff} is the blackbody temperature required to produce a TSI of 1361 Wm^{-2} at 1 AU and is representative of the mean opacity weighted radiative flux. Figure 3 shows the relative irradiance contributions for the active Sun to quiet Sun transition for the four integrated bands defined in Figure 2 and for the time period 04/2004 to 02/2008. This is done for both the SORCE observations (shown in light gray) and for the daily model runs described by *Lean* [2000]. The daily solar flux data used for this study is available at http://www.geo.fu-berlin.de/en/met/ag/strat/research/SOLARIS/Input_data/index.html. The ~0.5 W m^{-2} change in TSI based on the SIM observations is composed of nearly compensating trends in spectral irradiance with the 200–400 nm region slightly outweighing the trends in the mid-

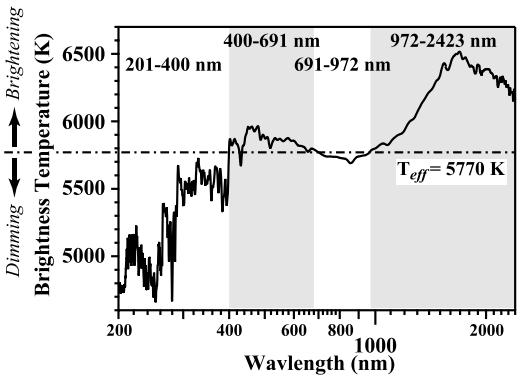

Figure 2. The SIM brightness temperature (T_b) is shown as a function of wavelength. The expected SSI variability is partitioned according to its location relative to the effective solar temperature (T_{eff}) of 5770 K as determined from the TSI. Wavelengths where $T_b < T_{eff}$ show a dimming with decreasing solar activity (corresponding to Figures 1b, 1c, and 1e), whereas the wavelengths with $T_b > T_{eff}$ show a brightening with decreasing solar activity (corresponding to Figures 1d, 1f, and 1g).

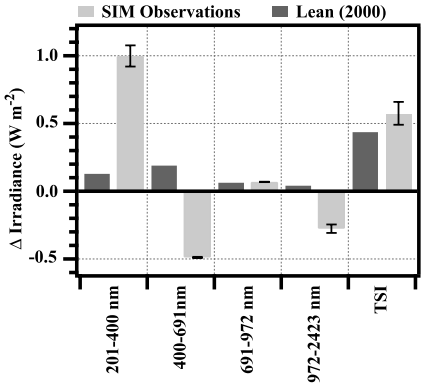

Figure 3. Compared are the measured and modeled SSI variability. The bar chart compares the irradiance change during the 04/2004–2/2008 time frame relative to the 11/2007 solar minimum reference for both the *Lean* [2000] model and the SORCE SIM. The spectra are decomposed into the same spectral bands defined in Figure 2. For the SORCE 680–970 nm bin, the change in irradiance is estimated to be the contribution without the suppression from the active regions evident in the April– August 2004 time frame. The error bars on this plot are representative of the errors associated with SIM photometric precision and estimated contributions due to degradation. Integrated over the full wavelength coverage of the instrument, these errors account for about 40% of the 170 parts per million fractional difference from the TIM TSI (the value shown in the fifth position of this graph but with the estimated SIM error bars). The other sources of uncertainty are most likely due to low grade imprecision associated with detector sensitivity changes with temperature and aliasing due to different sampling schemes for TSI and SSI. For comparative purposes, the solar cycle 23 minimum to maximum TSI change is approximately 1.3 Wm^{-2}.

visible and infrared spectral regions. This behavior is in contrast to the model estimate showing all bands decrease with decreasing solar activity, with the 400–691 nm spectral region accounting for ~44% of the TSI change. It is very important to note that these observations indicate significantly larger variability in the ultraviolet, by almost a factor of 10 in the 200–400 nm range over the model that was based on UARS ultraviolet observations [*Lean et al.*, 1997]. For the UARS study, the variability is best known for wavelengths less than 250 nm where it is much larger and less uncertain than for wavelengths longer than 250 nm — except near the more variable chromospheric emissions at 280 nm (Mg II) and 393 nm (Ca II). A model for the visible and near infrared was performed with a 3-component solar atmosphere model that accounts for the quiet sun and relative areas of sunspot and facular areas on the solar disk based on the findings of *Solanki and Unruh* [1998]. This model also predicts a negative solar cycle trend in the neighborhood of the H- opacity minimum at 1632 nm that is consistent with some observations [*Moran et al.*, 1992], but its contribution is not significant over the broader 971-2423 nm band. Note, however, that in the SIM observations this trend is negative throughout the 971-2423 nm range. Other recent solar spectral irradiance models such as SATIRE [*Krivova et al.*, 2006] indicate larger variability in the 300–400 nm range that are in closer agreement to the SIM observations, and detailed comparative studies are needed to define the level of agreement over longer time scales; comparisons with this model over solar rotational time scales have already been performed [*Unruh et al.*, 2008]. Likewise, the data from the *Lean* [2000] model has been compared with both the SORCE SIM and TIM instruments [*Lean et al.*, 2005] and is a frequently used for Earth climate studies.

3. Discussion

[6] The long-term spectral irradiance trends observed by SIM are consistent with a temperature gradient in the photosphere that, on average, is slightly shallower during the peak of solar activity than it is under quiet conditions as illustrated in Figure 4 [*Fontenla et al.*, 2006, 2007] for quiet sun and facula in the neighborhood of T_{eff}. This is consistent with a slightly higher temperature at the top of the photosphere that increases irradiance at some wavelengths during solar maximum and a slightly lower temperature at the bottom of the photosphere that induces dimming at other wavelengths. This effect might be explained by a slight reduction of the Rosseland mean opacity [*Mihalas*, 1978] in

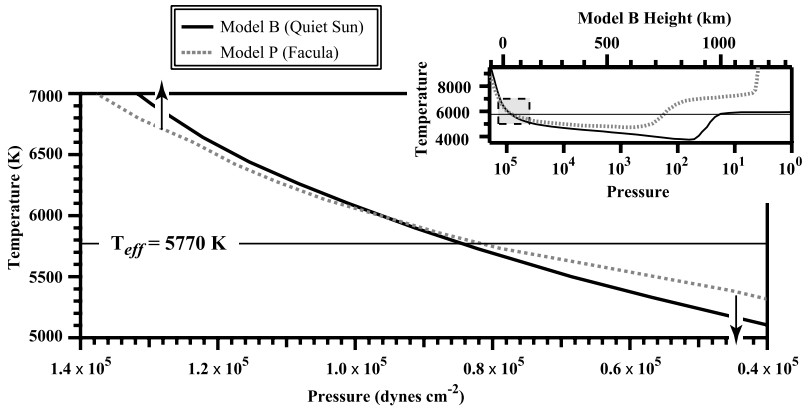

Figure 4. Solar atmosphere temperature profiles are shown for quiet sun and facula. The detail at the upper right shows the structure of the atmospheric temperature profiles throughout the photosphere and chromosphere, and the main graph shows an expanded view of the photospheric temperature profile in the neighborhood of T_{eff}. As the sun becomes less active, the temperature profile of facular regions tends to move in the direction indicated by the arrows.

the photosphere during solar maximum, or from a slightly increased mechanical energy transport through the photosphere, for instance, by magnetic free-energy flow [*Trujillo Bueno et al.*, 2004] or by convective motions [*Henoux and Somov*, 1991]. While SIM observations cannot identify the mechanism, they determine the photospheric temperature where opposing trends in spectral irradiance occur over periods of declining and ascending solar activity. This temperature was determined to be at slightly above T_{eff}. Further in-depth modeling (in preparation) will provide more details.

[7] Several recent observations of solar surface features are consistent with the SIM irradiance observations. Observations in both the 525–676 nm region [*Topka et al.*, 1997] and in the near-infrared [*Sánchez Cuberes et al.*, 2002] indicate that enhanced magnetic field regions show dimming relative to the quiet sun over most of the solar disk except when they are very close to the limb where they exhibit brightening [*Fontenla et al.*, 2004]. Thus, during times of increased solar activity (increased magnetic field) a decrease in irradiance at those wavelengths should be expected. While these analyses of solar images support the SIM observations, at the present time there is no direct validation through independent irradiance observations that have a physically based degradation correction [*Fröhlich et al.*, 1997; *Skupin et al.*, 2005]. Both the magnitude and the phase relations of the SIM observations rely on sensitive degradation corrections and further validation will occur during the onset of Solar Cycle 24 where the reversal of these trends is expected to occur.

[8] Earth-climate (global averaged surface temperature) response to irradiance variability over a solar-cycle is estimated to be about 0.1 K. Various possible mechanisms of climate response to solar variability have been identified and are dependent on wavelength [*Lean et al.*, 2005]. The direct heating of the Earth's surface is a consequence of absorption of solar irradiance in the near ultraviolet ($\lambda \geq$ 320 nm), visible, and near infrared. Radiation at shorter wavelengths is absorbed in the upper atmosphere and never reaches the surface. Solar variability in the ultraviolet part of the spectrum and its influence on ozone concentration is identified as an indirect response mechanism that affects climate through radiative and dynamic coupling between the stratosphere and troposphere. A non-linear mechanism is the alteration of internal modes of climate variability such as El Niño – Southern Oscillation (ENSO) and the North Atlantic Oscillation (NAO). Additionally, these mechanisms can induce regional changes that are larger than the globally averaged change [*Lean and Rind*, 2008].

[9] The climatic impact of the SORCE SIM observed variability in SSI is yet unknown because climate models have not been forced by this kind of variability. Spectral bands that vary out of phase with TSI will induce vertical and horizontal temperature gradients in ways that are not currently represented in models. For example, the mid-visible Chappuis ozone bands may play a larger role than previously considered because solar variability in that visible spectral region is at times out of phase with the ultraviolet spectral region. This could, in part, explain some of the vertical ozone response to solar forcing in the lower stratosphere that cannot be explained by current models [*Hood*, 2003]. It is critical that these new solar spectral variability results from SIM be included in climate models to understand the potential direct and indirect consequences to climate change.

[10] **Acknowledgments.** We wish to thank Judith Lean at the Naval Research Laboratory for providing the model output used for this study and Gregory Kopp at LASP for discussions on the TSI measurements. This research was supported by NASA contract NAS5-97045. Correspondence and requests for materials should be addressed to J.W.H. (jerald.harder@lasp.colorado.edu).

References

Fontenla, J. M., J. Harder, G. Rottman, T. N. Woods, G. M. Lawrence, and S. Davis (2004), The signature of solar activity in the infrared spectral irradiance, *Astrophys. J.*, *605*, L85.

Fontenla, J. M., E. Avrett, G. Thuillier, and J. Harder (2006), Semiempirical models of the solar atmosphere. I. The quiet- and active Sun photosphere at moderate resolution, *Astrophys. J.*, *639*, 441, doi:10.1086/499345.

Fontenla, J. M., K. S. Balasubramaniam, and J. Harder (2007), Semiempirical models of the solar atmosphere. II. The quiet Sun low chromosphere at moderate resolution, *Astrophys. J.*, *667*, 1243, doi:10.1086/520319.

Forster, P., et al. (2007), Changes in atmospheric constituents and in radiative forcing, in *Climate Change 2007: The Physical Science Basis. Contribution of Working Group I to the Fourth Assessment Report of the Intergovernmental Panel on Climate Change*, edited by S. Solomon et al., p. 129, Cambridge Univ. Press, Cambridge, U. K.

Fröhlich, C. (2006), Solar irradiance variability since 1978 revision of the PMOD composite during solar cycle 21, *Space Sci. Rev.*, *125*, 53.

Fröhlich, C., et al. (1997), The first results from SOHO, *Sol. Phys.*, *170*, 1.

Haigh, J. D. (1994), The role of stratospheric ozone in modulating the solar radiative forcing of climate, *Nature*, *370*, 544.

Harder, J., J. Fontenla, O. R. White, G. Rottman, and T. N. Woods (2005), Solar spectral irradiance variability comparisons of the SORCE SIM instrument with monitors of solar activity and spectral synthesis, *Mem. Soc. Astron. Ital.*, *76*, 735.

Henoux, J. C., and B. V. Somov (1991), The photospheric dynamo, *Astron. Astrophys.*, *241*, 613.

Hood, L. L. (2003), Thermal response of the tropical tropopause region to solar ultraviolet variations, *Geophys. Res. Lett.*, *30*(23), 2215, doi:10.1029/2003GL018364.

Kopp, G., G. Lawrence, and G. Rottman (2005), The Total Irradiance Monitor (TIM): Science results, *Sol. Phys.*, *230*, 129.

Krivova, N. A., S. Solanki, and L. Floyd (2006), Reconstruction of solar UV irradiance in cycle 23, *Astron. Astrophys.*, *452*, 631.

Labitzke, K., J. Austin, N. Butchart, J. Knight, M. Takahashi, M. Nakamoto, T. Nagashima, J. Haigh, and V. Williams (2002), The global signal of the 11-year solar cycle in the stratosphere: Observations and models, *J. Atmos. Sol. Terr. Phys.*, *65*, 203.

Lean, J. (1991), Variations in the Sun's radiative output, *Rev. Geophys.*, *29*, 505.

Lean, J. (2000), Evolution of the Sun's spectral irradiance since the Maunder minimum, *Geophys. Res. Lett.*, *27*, 2425.

Lean, J. L., and D. H. Rind (2008), How natural and anthropogenic influences alter global and regional surface temperatures: 1889 to 2006, *Geophys. Res. Lett.*, *35*, L18701, doi:10.1029/2008GL034864.

Lean, J. L., G. J. Rottman, H. L. Kyle, T. N. Woods, J. R. Hickey, and L. C. Puga (1997), Detection and parameterization of variations in solar mid- and near-ultraviolet radiation (200–400 nm), *J. Geophys. Res.*, *102*, 29,939.

Lean, J., G. Rottman, J. Harder, and G. Kopp (2005), SORCE contributions to new understanding of global change and solar variability, *Sol. Phys.*, *230*, 27.

London, J., G. J. Rottman, T. N. Woods, and F. Wu (1993), Time variations of solar UV irradiance as measured by the SOLSTICE (UARS) instrument, *Geophys. Res. Lett.*, *20*, 1315.

Mihalas, D. (1978), *Stellar Atmospheres*, 76 pp., W. H. Freeman, San Francisco, Calif.

Moran, T., P. Foukal, and D. Rabin (1992), A photometric study of faculae and sunspots between 1.2 and 1.6 μm, *Sol. Phys.*, *142*, 35.

Rottman, G., J. Harder, J. Fontenla, T. N. Woods, O. R. White, and G. Lawrence (2005), The Spectral Irradiance Monitor (SIM): Early observations, *Sol. Phys.*, *230*, 205.

Sánchez Cuberes, M., M. Vázquez, J. A. Bonet, and M. Sobotka (2002), Infrared photometry of solar photospheric structures. II. Center-to-limb variation of active regions, *Astrophys. J.*, *570*, 886.

Skupin, J., S. Noel, M. W. Wuttke, M. Gottwald, H. Bovensmann, M. Weber, and J. P. Burrows (2005), SCIAMACHY solar irradiance observation in the spectral range from 240 to 2380 nm, *Adv. Space Res.*, *35*, 370.

Solanki, S. K., and Y. C. Unruh (1998), A model of the wavelength dependence of solar irradiance variations, *Astron. Astrophys.*, *329*, 747.

Topka, K. P., T. D. Tarbell, and A. M. Title (1997), Properties of the smallest solar magnetic elements. II. Observations versus hot wall models of faculae, *Astrophys. J.*, *484*, 479.

Trujillo Bueno, J., N. Shchukina, and A. Asensio Ramos (2004), A substantial amount of hidden magnetic energy in the quiet Sun, *Nature*, *430*, 326.

Unruh, Y. C., N. Krivova, S. Solanki, J. Harder, and G. Kopp (2008), Spectral irradiance variations: Comparisons between observations and the SATIRE model on solar rotation time scales, *Astron. Astrophys.*, *486*, 311, doi:10.1051/0004-6361:20078421.

Willson, R. C., and A. V. Mordvinov (2003), Secular total solar irradiance trend during solar cycles 21–23, *Geophys. Res. Lett.*, *30*(5), 1199, doi:10.1029/2002GL016038.

J. W. Harder, J. M. Fontenla, P. Pilewskie, E. C. Richard, and T. N. Woods, Laboratory for Atmospheric and Space Physics, University of Colorado, Campus Box 590, Boulder, CO 80303, USA. (jerald.harder@lasp.colorado.edu)